



## OPEN ACCESS

## EDITED BY

Kim Meow Liew,  
City University of Hong Kong, Hong  
Kong, SAR China

## REVIEWED BY

Chenggao Li,  
Harbin Institute of Technology, China  
Ionut Ovidiu Toma,  
Gheorghe Asachi Technical University of  
Iasi, Romania

## \*CORRESPONDENCE

Huaxin Liu,  
✉ lgliuhuaxin@163.com

RECEIVED 10 April 2024

ACCEPTED 26 June 2024

PUBLISHED 19 July 2024

## CITATION

Yang W, Liu H and Wang H (2024),  
Experimental study on mechanical properties  
of basalt fiber reinforced nano-SiO<sub>2</sub> concrete  
after high temperature.  
*Front. Mater.* 11:1415144.  
doi: 10.3389/fmats.2024.1415144

## COPYRIGHT

© 2024 Yang, Liu and Wang. This is an  
open-access article distributed under the  
terms of the [Creative Commons Attribution  
License \(CC BY\)](https://creativecommons.org/licenses/by/4.0/). The use, distribution or  
reproduction in other forums is permitted,  
provided the original author(s) and the  
copyright owner(s) are credited and that the  
original publication in this journal is cited, in  
accordance with accepted academic practice.  
No use, distribution or reproduction is  
permitted which does not comply with  
these terms.

# Experimental study on mechanical properties of basalt fiber reinforced nano-SiO<sub>2</sub> concrete after high temperature

Weidong Yang, Huaxin Liu\* and Hesong Wang

College of Civil and Architectural Engineering, Liaoning University of Technology, Jinzhou, China

In enhancing the high-temperature resistance of concrete, incorporating fiber materials was established as an effective approach. This study focused on evaluating the cubic compressive strength, splitting tensile strength, prism compressive strength, and flexural strength of plain concrete, nano-SiO<sub>2</sub> concrete, and basalt fiber nano-SiO<sub>2</sub> concrete when subjected to elevated temperatures. Subsequently, a concrete strength prediction model was established, and a microstructure analysis of the specimens was conducted. The results indicated that after exposure to 800°C, the cubic compressive strength, splitting tensile strength, prism compressive strength, and flexural strength of basalt fiber-reinforced nano-SiO<sub>2</sub> concrete increased by 33.7%, 15.6%, 10.4%, and 17.2%, respectively, compared to plain concrete. Furthermore, the fitting values of the strength prediction model were all above 0.9. Microstructure analysis revealed that the filling effect of nano-SiO<sub>2</sub> made the concrete matrix denser, while the basalt fiber effectively restrained the formation of cracks in the concrete matrix. Additionally, nano-SiO<sub>2</sub> promoted the formation of hydrated calcium silicate from Ca(OH)<sub>2</sub>(CH) and adhered to the basalt fiber, enhancing bonding and reducing the risk of concrete spalling.

## KEYWORDS

basalt fiber, nano-SiO<sub>2</sub> concrete, high temperature, mechanical property, microstructure

## 1 Introduction

Since its introduction in 1830, concrete, as the most prevalent artificial material, has played a crucial role in the development and progress of human society (Forty, 2012). In recent years, China has witnessed a gradual acceleration in urbanization. The increasing population density has led to a surge in the construction of high-rise and super high-rise buildings. Concurrently, the incidence of building fires has become more frequent. In the event of a fire, elevated temperatures can significantly compromise the stability of the internal structure of concrete. Concrete structures are susceptible to spalling, leading to a rapid reduction in structural bearing capacity, increased peak strain, and substantial durability loss. These factors pose a serious threat to the safety of building structures (Wang et al., 2012; Zhang et al., 2019). Consequently, enhancing the high-temperature resistance of concrete has become a topic of increasing concern among scholars.

Research demonstrated that incorporating fiber into concrete effectively enhanced its high-temperature resistance. Commonly utilized types included basalt fiber (BF) (Sim et al., 2005; High et al., 2015; Piao, 2017; Qiu et al., 2019; Zhao et al., 2019; Rong et al., 2020;

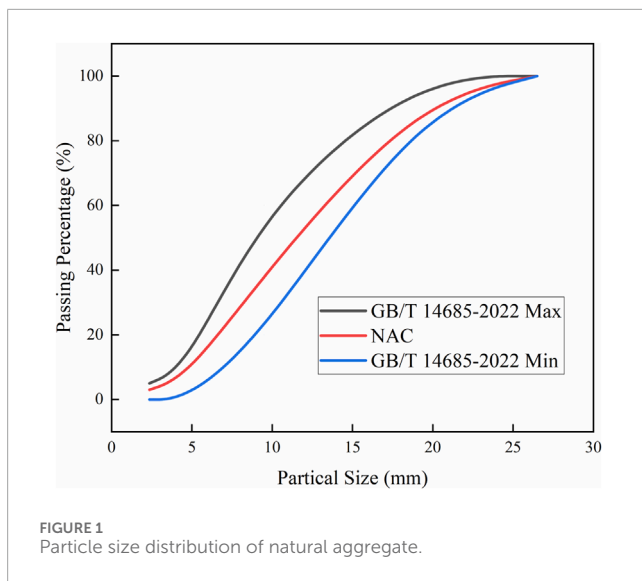
Qin, 2021), carbon fiber (Li and Xian, 2019; Lal et al., 2022), and glass fiber (Mastali et al., 2016). Due to the elevated cost of carbon fiber (Swolfs et al., 2014), while glass fiber was prone to breakage and could be challenging to uniformly disperse within the concrete matrix (Mastali et al., 2016). In contrast, basalt fiber exhibited notable characteristics, including a large elastic modulus, high resistance to high temperatures, low resistance to low temperatures, corrosion resistance, and favorable cost performance (Huang et al., 2006). This characteristic enabled BF to play a significant role in crack resistance under elevated temperatures, consequently contributing to the improvement of both the compressive and tensile properties of concrete after exposure to high temperatures. The study of Alaskar et al. (2021) concluded that, at 300°C, the compressive strength and tensile strength of BF concrete with a BF volume content of 1.0% were 30.3 MPa and 2.3 MPa, respectively. These values were notably higher compared to ordinary concrete at the same temperature, which exhibited compressive and tensile strengths of 26.6 MPa and 1.3 MPa, respectively. Yang et al. (2023) suggest that, upon heating BF concrete to 800°C, the proportion of tensile cracks in ordinary concrete specimens progressively decreased from 81.28% to 39.18%, while the proportion of shear cracks increased from 18.72% to 60.82%. In specimens with a BF volume content of 0.26%, the proportion of tensile cracks decreased from 86.39% to 45.74%, and the proportion of shear cracks increased from 13.61% to 54.26%. Due to the similar material properties of BF and concrete, they exhibited better compatibility and were extensively studied in the field of civil engineering both domestically and internationally (Dias and Thaumaturgo, 2005; Ayub et al., 2014; Cheng and Li, 2017; Sun et al., 2018). In recent years, it was observed that while the incorporation of a single type of fiber could effectively enhance the high-temperature resistance of concrete, there were inherent limitations associated with this approach. When fiber-reinforced concrete was exposed to high temperatures, the bond between the fiber and the concrete matrix underwent significant damage, resulting in substantial deterioration.

Certain characteristics inherent to nanomaterials were not present in traditional materials (Uthaman et al., 2021). The integration of nanomaterials into concrete had the potential to enhance the internal structure of concrete, improve the bond between the concrete matrix and fiber, and consequently, enhance the high-temperature resistance of fiber-reinforced concrete (Nigam and Verma, 2023). The most prevalent nanomaterials included nano-SiO<sub>2</sub> (NS) (Mukharjee and Barai, 2014), nano-Al<sub>2</sub>O<sub>3</sub> (León et al., 2014), and nano-TiO<sub>2</sub> (Mohseni et al., 2016). NS possessed characteristics such as small particle size, large specific surface area, strong surface adsorption capacity, substantial surface energy, effective dispersion performance, and exhibited both pozzolanic and filling effects (Ling et al., 2019; Xiao et al., 2021; Abhilash et al., 2021). The reaction of NS and CH crystals to form C-S-H could make the mortar more uniform and dense, and effectively improve the mechanical properties of concrete (Sikora et al., 2018). Consequently, NS found widespread applications in fields such as rubber, plastics, ceramics, and chemical catalysis, among others (Lu et al., 2013). Given the feasibility of applying NS to cement-based materials, successive research was conducted on NS concrete (Cai et al., 2017; Norhasri et al., 2017; Li et al., 2018). In a study by Shih et al. (2006), the performance of NS on Portland cement composites was investigated. It was observed that incorporating an

appropriate amount of sol-state NS into the cement paste effectively enhanced its compressive strength. Specifically, at a content of 0.6%, the compressive strength demonstrated a significant increase of 43.8%. In a study conducted by Bastami et al. (2014), it was observed that NS had a positive impact on the strength of high-strength concrete and contributed to a reduction in mass loss. The research further indicated that the inclusion of NS led to an increase in the high-temperature spalling temperature by 100°C. In a study conducted by Yan and Xing (2013), it was observed that after heat treatment at 400°C, the compressive strength, splitting tensile strength, and flexural strength of steel fiber reinforced concrete with NS increased by 35.09%, 84.62%, and 87.23%, respectively, compared with ordinary concrete. Scanning electron microscopy (SEM) analysis revealed an increased density at the interface between the steel fiber and the mortar.

A novel composite material, referred to as fiber-reinforced nano-concrete, was generated by integrating fiber material and nano-material into traditional concrete. Fiber-reinforced nano-concrete served to compensate for the shortcomings of individual materials, enhancing the strength of concrete through a synergistic effect (Sun et al., 2023). In recent years, many scholars undertook a series of studies on the properties of fiber-reinforced nano-concrete. In a study conducted by Zhu and Ma (2016), experimental research revealed a notable enhancement in the tensile and compressive strength of concrete through the incorporation of NS and BF. The optimal combination was identified when the NS content accounted for 1.2% of the cementitious material, and the BF volume content was 3 kg/m<sup>3</sup>. Wang et al. 2019 concluded, based on experiments and microstructure analysis, that the addition of BF and NS could enhance the performance of the interfacial transition zone and improve the high-temperature resistance of recycled concrete. In a study conducted by Zheng et al. (2021), the mixed application of NS and BF was investigated through experiments. NS was observed to enhance the bond between the fiber and matrix through coupling, thereby effectively improving the fiber reinforcement effect and enhancing the durability of recycled concrete. In summary, the incorporation of both fiber materials and nanomaterials into concrete demonstrated a positive effect on improving the physical and mechanical properties of the concrete.

In recent years, the frequent occurrence of fires intensified the demand for enhanced fire resistance in engineering structures. While existing studies primarily concentrated on the mechanical properties of fiber-nanomaterial composite reinforced concrete at 20°C, there was a scarcity of research on the high-temperature performance of concrete structures after exposure to high temperature. Moreover, investigations into the post-high-temperature performance predominantly centered on the properties of steel fiber and nanomaterial composite reinforced concrete. Research on the mechanical properties of concrete reinforced with other fiber and nanomaterial composites after exposure to high temperatures was still at an early stage. Therefore, this paper delved into the examination of the influence on cubic compressive strength, splitting tensile strength, prism compressive strength, and flexural strength of BF-reinforced NS concrete after exposure to high temperatures, along with an analysis of the microstructure. This study aimed to offer a theoretical foundation for the application of fiber materials and nanomaterials in concrete.



## 2 Experimental programs

### 2.1 Materials

The test utilized P.O 42.5 Portland cement. In accordance with the Chinese GB/T 14685-2022 standard (Zhang and Xie, 2022), natural coarse aggregate (NAC) with continuous gradation ranging from 5 mm to 20 mm was employed, and the particle size distribution is depicted in Figure 1. The fine aggregate comprised ordinary river sand with a fineness modulus of 2.53, categorizing it as medium sand in zone II. Main parameters of BF outlined in Table 1. NS is a specialized product for concrete, and its primary parameters are presented in Table 2. Ordinary tap water served as the water component. The appearance of BF and NS in this study is illustrated in Figure 2.

### 2.2 Mix design

The experiment considered the impact of varying fiber content and temperature fluctuations on the cubic compressive strength, splitting tensile strength, prism compressive strength, and flexural strength of BF-NS concrete. The BF content was set at 0.10%, 0.15%, and 0.20%, and incorporated into the concrete based on the volume percentage algorithm. NS was added to the concrete at a content of 1.0% of the total mass of cementitious materials instead of cement (Ashokan et al., 2023). Drawing from the existing research by scholars on concrete post-high temperature (Zhao et al., 2019; Zhang et al., 2023), the experiment was designed with five temperature levels: 20°C (control group), 200°C, 400°C, 600°C, and 800°C. Five experimental groups were established accordingly. The design test grouping and mix proportions are detailed in Table 3, adhering to the specifications outlined in the Chinese JGJ55-2011 standard (Ding and Leng, 2011). The numerical values following NS indicate the NS content, while the numerical values following BF represent the BF content.

### 2.3 Methods of test

In this test, the dimensions of the cubic compressive test specimen and the splitting tensile test specimen were 100 mm × 100 mm × 100 mm; the prism compression test specimen had a size of 100 mm × 100 mm × 300 mm, while the flexural test specimen measured 100 mm × 100 mm × 400 mm. The selection of concrete test block sizes in the test adhered to the guidelines of the Chinese CECS13:2009 standard (Huang and Zhao, 2010). A total of 300 specimens were prepared for the cubic compressive strength, splitting strength, prism compressive strength, and flexural strength tests at different temperatures, with 75 specimens (3 for each group) per test. After 24 h of curing, the molds were removed, and the specimens were placed in a standard curing room with a temperature of (20 ± 2)°C and a relative humidity of over 95% for 28 days. Subsequently, the specimens were transferred to a ventilated and dry environment, where they stood for 7 days to ensure the complete drying of the concrete specimens, preventing potential spalling during the high-temperature test. Finally, the high-temperature test was conducted using a box resistance furnace (SX2-12-10), as depicted in Figure 3. Target temperatures for the test were set at 200°C, 400°C, 600°C, and 800°C. The specimen was placed in a high-temperature furnace and heated to the target temperature at a rate of 10°C/min. The temperature-time curve of the specimen is measured using a K-type thermocouple, as illustrated in Figure 4. In line with previous research on concrete testing after exposure to high temperatures (Zhang et al., 2023), once the target temperature is attained within the resistance furnace, it is maintained at that level for a duration of 2 h. This ensures uniform heating of the concrete specimens both internally and externally. Subsequently, the specimen was removed and allowed to cool naturally to 20°C. Mechanical properties were tested in accordance with the Chinese GB/T 50081-2002 standard (Rong et al., 2002).

The microstructure of the fractured concrete surface and fibers was analyzed using scanning electron microscopic (ZEISS GeminiSEM 300, Germany). All scanning electron microscopy specimens were collected from the fracture sections obtained during the splitting tensile test of concrete subjected to high temperatures. Prior to scanning, the concrete samples underwent a vacuum process and were coated with a conductive layer using a Quorum SC7620 sputtering coating instrument. Subsequently, SEM analysis was conducted.

## 3 Results and discussion

### 3.1 Concrete mass loss

The test results of the mass loss rate of the specimen after different high temperatures are shown in Table 4. Figure 5 depicts the curve of the mass loss rate of each group of concrete with the change in temperature. The mass loss rate was measured by the specimen with the size of 100 mm × 100 mm × 100 mm. The mass loss rate decreased rapidly after 200°C–400°C, and the mass loss rate at 400°C was 5.41%–6.12%. The main reason was that the evaporation of bound water in concrete and the decomposition of CH crystal reduced part of the mass. The

TABLE 1 Main technical specifications of BF.

Diameter ( $\mu\text{m}$ )	Length (mm)	Density ( $\text{g}\cdot\text{cm}^{-3}$ )	Tensile strength (MPa)	Elastic modulus (GPa)	Elongation at break (%)
16	12	2.73	3,250	95	3.2

TABLE 2 Main technical indicators of NS.

Appearance	Particle size (nm)	Specific surface area ( $\text{m}^2/\text{g}$ )	Purity (%)	pH	Loss on ignition (%)
White powder	25	$150 \pm 30$	$\geq 99.5$	5~7	$\leq 6.0$

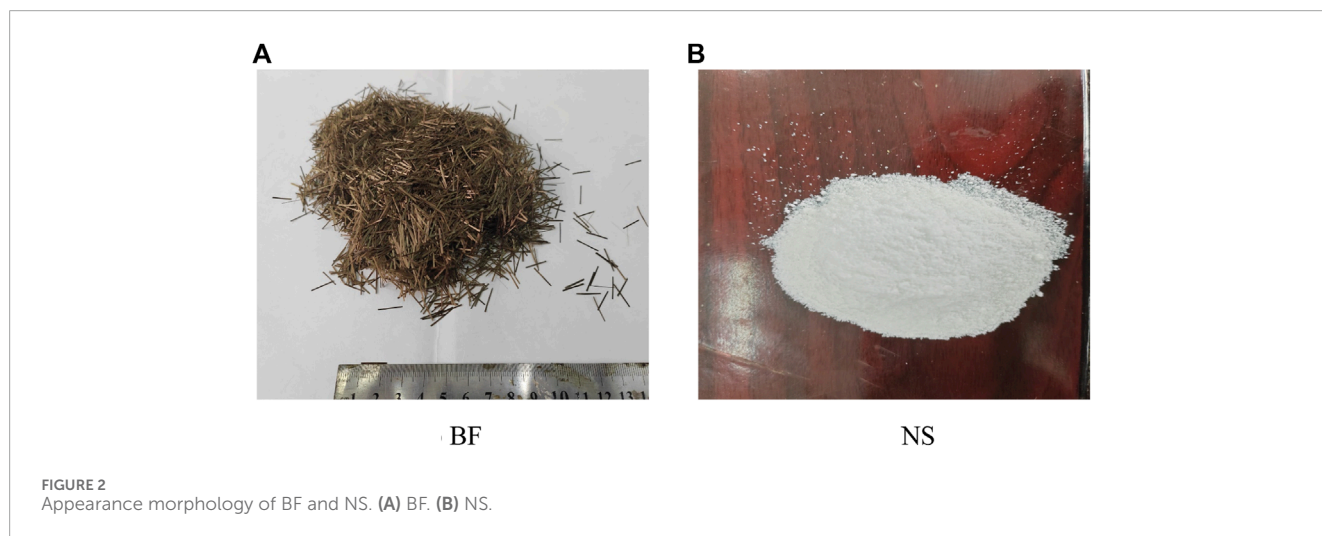


TABLE 3 Concrete mix ratio.

Label	NS (%)	BF (%)	Cement ( $\text{kg}\cdot\text{m}^{-3}$ )	Sand ( $\text{kg}\cdot\text{m}^{-3}$ )	NCA ( $\text{kg}\cdot\text{m}^{-3}$ )	Water ( $\text{kg}\cdot\text{m}^{-3}$ )
NS0	—	—	427	650	1,027	210
NS1-B0	1	0	422.73	650	1,027	210
NS1-B0.1	1	0.10	422.73	650	1,027	210
NS1-B0.15	1	0.15	422.73	650	1,027	210
NS1-B0.2	1	0.20	422.73	650	1,027	210

mass loss rate at 600°C ranged from 6.53% to 7.37%, primarily attributed to the decomposition of C-S-H gel in concrete. This decomposition led to the generation of gas and evaporation, resulting in a decline in concrete quality. Subsequently, at 800°C, the mass loss rate increased to a range of 7.86%–9.44%, mainly due to the decomposition of hydration products in concrete following exposure to high temperatures. This decomposition further led to a decrease in concrete strength and spalling.

### 3.2 Cubic compressive strength

The cubic compressive strength test results of the specimens after exposure to different high temperatures are presented in Table 4. Figures 6A,B illustrate the variation in cubic compressive strength and cubic compressive strength residual rate for each concrete group with temperature. Observing Figures 6A,B reveal that, excluding plain concrete, the cubic compressive strength of



FIGURE 3 Box-type resistance furnace.

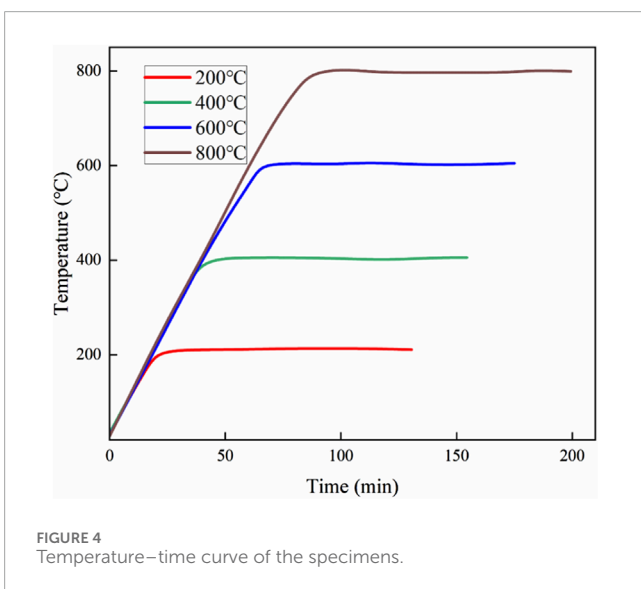


FIGURE 4 Temperature–time curve of the specimens.

each concrete group generally follows an initial increase followed by a subsequent decrease with rising temperature. Between 20°C and 400°C, there was a noticeable but relatively small increase in cubic compressive strength, with an approximate range of 0.6%–2.6%. The increase in cubic compressive strength between 20°C and 400°C was attributed to the hydration reaction of evaporated free water and void water with unreacted cement particles, enhancing the compressive strength of the concrete cubic. However, beyond 400°C, the cubic compressive strength of each concrete group exhibited a declining trend compared to 20°C. Following exposure to high temperatures of 600°C and 800°C, the strength decreased by 16.0%–22.8% and 47.4%–59.2%, respectively. This decline was mainly attributed to the gradual decomposition of the hydration products of concrete after 400°C, leading to a decrease in cubic compressive strength.

The addition of NS enhanced the cubic compressive strength of concrete. After exposures to temperatures of 20°C, 200°C, 400°C, 600°C, and 800°C, the cubic compressive strength increased by

9.7%, 13.5%, 16.6%, 12.2%, and 7.9%, respectively, compared to plain concrete. This improvement was primarily attributed to the pozzolanic and filling effects of NS, which increased the density of the cement matrix, consequently boosting the strength. At 20°C, the cubic compressive strength of BF-NS concrete with 0.10% and 0.15% fiber content increased by 4.9% and 3.8%, respectively, compared with NS concrete; at 200°C, it increased by 3.9% and 3.2%; at 400°C, it increased by 4.6% and 3.3%; at 600°C, it increased by 13.6% and 10.6%; at 800°C, it increased by 28.3% and 33.7%. This improvement was mainly attributed to the fact that BF formed a fiber network inside the concrete, filling and bridging the voids and micro-cracks, thereby enhancing the strength of NS concrete. The incorporation of BF at a content of 0.20% exerted an adverse effect on the cubic compressive strength of NS concrete. At each temperature, the cubic compressive strength was lower compared to that of NS concrete. This decline was attributed to the occurrence of agglomeration during the mixing process when the BF content was excessively high. This phenomenon led to the presence of a substantial amount of air within the concrete, constituting a significant factor contributing to the decrease in cubic compressive strength.

It is observed from Figure 6B that, with the increase in temperature, the residual rate of cubic compressive strength for each concrete group follows a similar trend to that of cubic compressive strength. Apart from plain concrete, there was a noticeable pattern of an initial increase followed by a subsequent decrease. Under various temperature conditions, the inclusion of 0.10% and 0.15% BF content enhanced the residual rate of cubic compressive strength for concrete. At 200°C, the residual compressive strength of concrete cubes in each group, except plain concrete, reached its peak, measuring 102.7%, 101.7%, 102.1%, and 102.0%, respectively. After 400°C, the compressive strength residual rate of concrete cubes in each group began to decrease, reaching its minimum at 800°C, with values of 41.5%, 40.8%, 50.0%, 52.5%, and 43.3%, respectively. The residual rate of cubic compressive strength after adding BF to concrete was significantly higher than that of ordinary concrete and NS concrete. This was because BF had high thermal conductivity, effectively transferring heat to the interior of concrete and reducing the temperature gradient.

By comparing the cubic compressive strength of each group of concrete after exposure to high temperatures with the cubic compressive strength at 20°C, the relationship curve of the cubic compressive strength ratio with temperature was obtained. As shown in Figure 6C and Eqs (1–5), the fitting relationship between the compressive strength ratio of each group of concrete cubes and temperature is obtained:

$$NS0: f_C^T / f_C = 99.63 + 0.009T - 1.09 \times 10^{-5}T^2 - 1.35 \times 10^{-7}T^3 R^2 = 0.997 \quad (1)$$

$$NS1 - B0: f_C^T / f_C = 98.61 + 0.05T - 9.16 \times 10^{-5}T^2 - 7.66 \times 10^{-8}T^3 R^2 = 0.986 \quad (2)$$

$$NS1 - B0.1: f_C^T / f_C = 99.42 + 0.018T + 1.27 \times 10^{-5}T^2 - 1.42 \times 10^{-7}T^3 R^2 = 0.995 \quad (3)$$

$$NS1 - B0.15: f_C^T / f_C = 99.32 + 0.025T - 1.62 \times 10^{-5}T^2 - 1.1 \times 10^{-7}T^3 R^2 = 0.996 \quad (4)$$

TABLE 4 Mechanical properties of concrete.

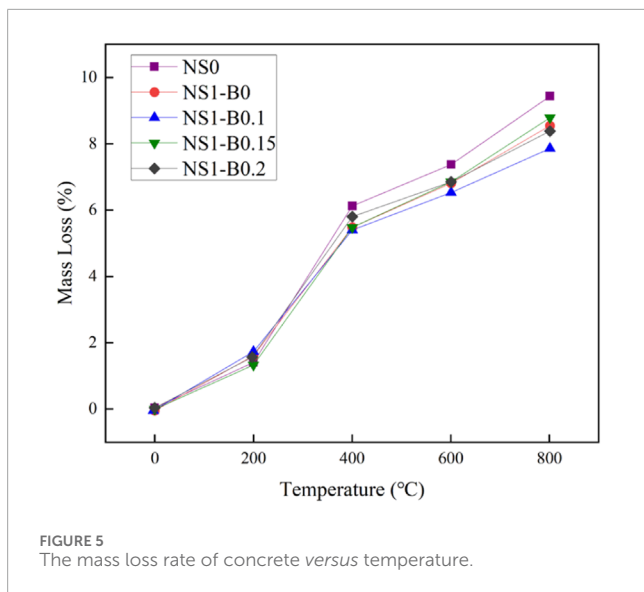
Label	Temperature (°C)	Mass loss (%)	Cubic compressive strength (MPa)	Splitting tensile strength (MPa)	Prism compressive strength (MPa)	Flexural strength (MPa)
NS0	20	0	41.1	3.44	31.2	4.48
	200	1.41	40.8	3.07	29.2	4.18
	400	6.12	39.1	2.83	26.3	3.10
	600	7.37	31.1	1.81	20.4	1.92
	800	9.44	17.1	0.95	15.2	1.62
NS1-B0	20	0	45.1	3.71	36.6	5.26
	200	1.61	46.3	3.36	35.0	4.97
	400	5.48	45.6	2.96	31.7	4.18
	600	6.81	34.9	1.84	24.2	2.76
	800	8.55	18.4	0.89	18.3	1.98
NS1-B0.1	20	0	47.3	3.82	38.6	5.04
	200	1.73	48.1	3.37	36.8	4.56
	400	5.41	47.7	3.13	33.8	3.81
	600	6.53	39.6	2.11	26.4	2.31
	800	7.86	23.6	1.11	20.2	1.82
NS1-B0.15	20	0	46.8	4.04	37.9	5.11
	200	1.33	47.8	3.57	36.4	4.67
	400	5.51	47.1	3.16	33.1	4.00
	600	6.85	39.3	2.13	25.8	2.41
	800	8.79	24.6	1.02	19.5	1.89
NS1-B0.2	20	0	44.3	3.86	37.1	5.07
	200	1.57	45.2	3.16	35.9	4.62
	400	5.79	44.6	3.03	32.4	3.78
	600	6.87	34.2	1.83	24.8	2.23
	800	8.38	19.2	0.91	19.0	1.80

$$NS1 - B0.2: f_C^T / f_C = 98.58 + 0.048T - 9.84 \times 10^{-5}T^2 - 6.09 \times 10^{-8}T^3 R^2 = 0.980 \tag{5}$$

Where  $f_C^T$  (MPa) is the cubic compressive strength of concrete after action temperature,  $f_C$  (MPa) is the cubic compressive strength of concrete at 20°C,  $T$  (°C) is the temperature,  $R^2$  is the correlation coefficient.

### 3.3 Splitting tensile strength

The splitting tensile strength test results of the specimens after exposure to different high temperatures are presented in Table 4. Figures 7A,B illustrate the variation of splitting tensile strength and the residual rate of splitting tensile strength for each group of concrete with temperature. Observing Figures 7A,B reveals that,



with the increase in temperature, the splitting tensile strength of each group of concrete shows a gradual downward trend. After exposure to various temperatures, the splitting tensile strength of NS concrete was 7.8%, 9.4%, 6.0%, 12.2%, and 7.7% higher than that of plain concrete, respectively. This improvement was mainly attributed to the reaction between NS and CH crystals, which promoted the hydration of concrete, thereby increasing its strength. At 20°C, the splitting tensile strength of BF-NS concrete with BF content of 0.10%, 0.15%, and 0.20% was increased by 3.0%, 8.9%, and 4.0%, respectively, compared with that of NS concrete; at 200°C, it increased by 7.5%, 11.2%, and 5.6%; at 400°C, it increased by 6.5%, 7.8%, and 4.8%; at 600°C, it increased by 3.9%, 6.9%, and 2.5%; and at 800°C, it increased by 15.6%, 13.5%, and 7.3%. Under the action of tensile stress, the concrete matrix would disintegrate, and the bond loss between cement paste and aggregate would occur. The uniform incorporation of BF made the stress distribution inside the concrete matrix uniform, thus improving the splitting tensile strength of concrete. Especially at 800°C, the splitting tensile strength of NS concrete was significantly improved. Overall, at each temperature, the BF with a content of 0.15% had a notable effect on the splitting tensile strength of NS concrete.

It is observed from Figure 7B that the residual rate of splitting tensile strength decreases gradually with the increase in temperature, reaching the lowest at 800°C. The residual rate of splitting tensile strength of plain concrete was 27.6%, and that of NS concrete was 24.5%. At different temperatures, BF-NS concrete exhibited good tensile strength. The residual rate of splitting tensile strength of BF-NS concrete with 0.15% fiber content was 14.6% higher than that of NS concrete after 800°C. Due to the high melting point of BF, its susceptibility to the effects of high temperature was limited. This characteristic enabled BF to contribute to crack resistance and toughening under high temperatures, resulting in a higher residual rate of splitting tensile strength for concrete with BF compared to ordinary concrete and NS concrete.

Comparing the splitting tensile strength of each group of concrete after exposure to high temperatures with the splitting tensile strength at 20°C, the relationship curve of the splitting

tensile strength ratio with temperature was obtained. As shown in Figure 7C and Eqs (6–10), the fitting relationship between the splitting tensile strength ratio of each group of concrete and temperature is obtained:

$$\text{NS0: } f_C^T/f_C = 99.43 - 0.014T - 1.05 \times 10^{-4}T^2 + 1.18 \times 10^{-8}T^3 \quad R^2 = 0.952 \quad (6)$$

$$\text{NS1 - B0: } f_C^T/f_C = 99.36 + 3.9 \times 10^{-4}T - 1.72 \times 10^{-4}T^2 + 6.62 \times 10^{-8}T^3 \quad R^2 = 0.974 \quad (7)$$

$$\text{NS1 - B0.1: } f_C^T/f_C = 99.98 - 0.038T - 2.03 \times 10^{-5}T^2 - 5.45 \times 10^{-8}T^3 \quad R^2 = 0.960 \quad (8)$$

$$\text{NS1 - B0.15: } f_C^T/f_C = 101.60 - 0.086T + 1.47 \times 10^{-4}T^2 - 1.97 \times 10^{-7}T^3 \quad R^2 = 0.999 \quad (9)$$

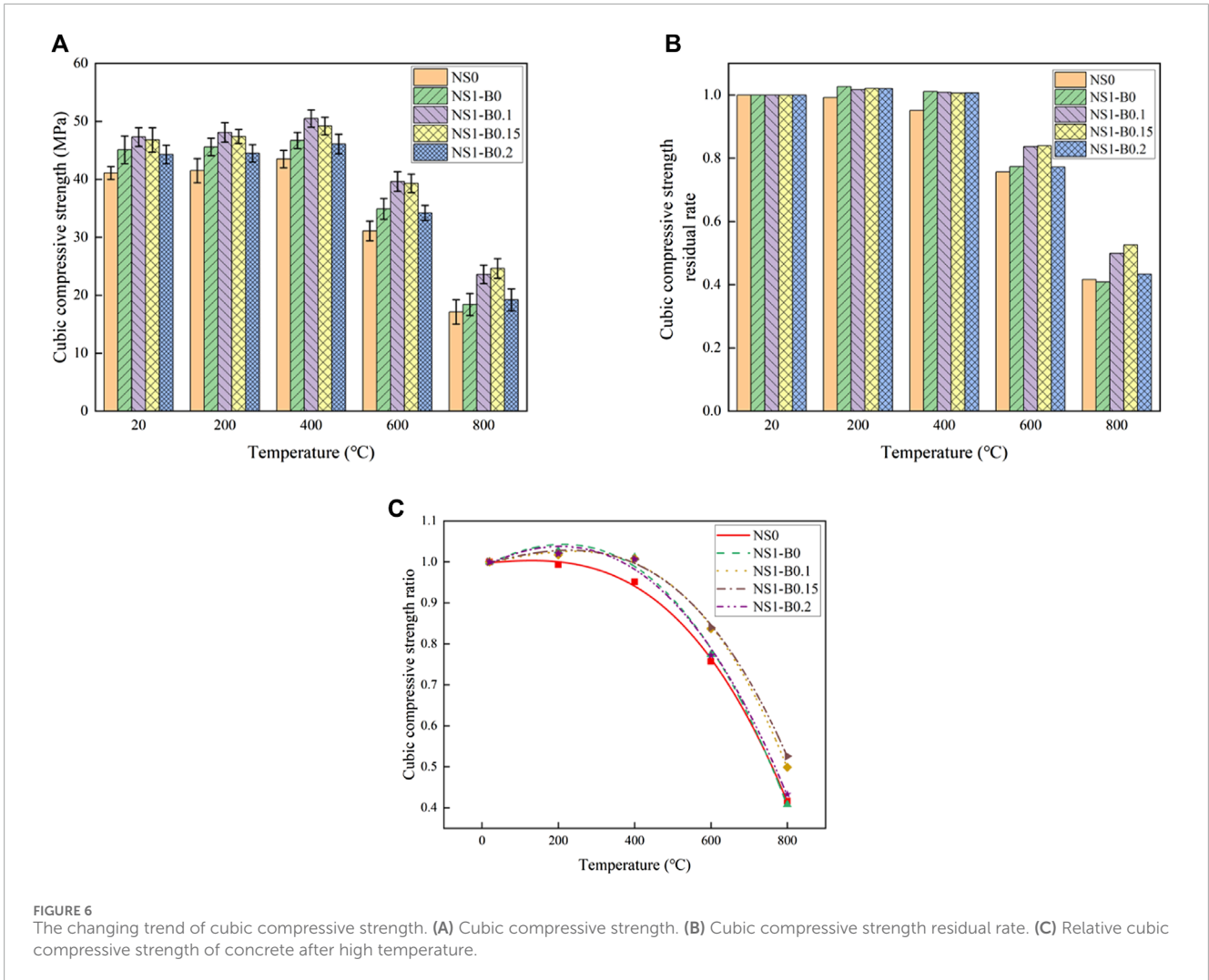
$$\text{NS1 - B0.2: } f_C^T/f_C = 100.10 - 0.071T + 3.44 \times 10^{-5}T^2 - 8.35 \times 10^{-8}T^3 \quad R^2 = 0.904 \quad (10)$$

Where  $f_C^T$  (MPa) is the splitting tensile strength of concrete after the action temperature,  $f_C$  (MPa) is the splitting tensile strength of concrete at 20°C,  $T$  (°C) is the temperature,  $R^2$  is the correlation coefficient.

### 3.4 Prism compressive strength

The prism compressive strength test results of the specimens after exposure to different high temperatures are presented in Table 4. Figures 8A,B illustrate the variation of prism compressive strength and prism compressive strength residual rate for each group of concrete with temperature. It can be observed from Figures 8A,B that, with the increase in temperature, the prism compressive strength of each group of concrete shows a gradual downward trend. After exposure to various temperatures, the prism compressive strength of NS concrete was 17.3%, 19.9%, 20.5%, 18.6%, and 20.4% higher than that of plain concrete, respectively. This was attributed to the fact that NS filled the internal voids of concrete and refined the pore structure, resulting in a higher strength of NS concrete than that of plain concrete at various temperatures. At 20°C, the prism compressive strength of BF-NS concrete with 0.10%, 0.15%, and 0.20% BF was 5.5%, 3.6%, and 1.4% higher than that of NS concrete; at 200°C, it increased by 5.1%, 4.0%, and 2.6%; at 400°C, it increased by 6.6%, 4.4%, and 2.2%; at 600°C, it increased by 9.1%, 6.6%, and 2.5%; at 800°C, it increased by 10.4%, 6.6%, and 3.8%. It could be seen that this was mainly because the addition of BF resisted the generation of lateral cracks in concrete, thus enhancing the prism compressive strength of concrete. Especially at 800°C, the prism compressive strength of NS concrete was significantly improved. Overall, at each temperature, the BF with a content of 0.1% had a notable effect on the prism compressive strength of NS concrete.

As shown in Figure 8B, under various temperature conditions, the residual rate of prism compressive strength decreases with the increase in temperature. At 800°C, the prism compressive strength residual rate of plain concrete was only 48.7%, and that of NS concrete was only 50%. At different temperatures, BF-NS concrete



exhibited good prism compressive capacity. After 800°C, the residual rate of prism compressive strength of BF-NS concrete with 0.1% content was 2.3% higher than that of NS concrete. The residual rate of prism compressive strength after adding BF to concrete was significantly higher than that of ordinary concrete and NS concrete. This improvement was attributed to the enhanced stability of BF at high temperatures, which contributed to improved bonding within the concrete matrix.

Comparing the prism compressive strength of each group of concrete after exposure to high temperatures with the prism compressive strength at 20°C, the relationship curve of prism compressive strength ratio with temperature was obtained. As shown in Figure 8C and Eqs (10–15), the fitting relationship between the prism compressive strength ratio of each group of concrete and temperature can be obtained:

$$NS0: f_C^T/f_C = 99.78 - 3.30 \times 10^{-4}T - 1.30 \times 10^{-4}T^2 + 6.28 \times 10^{-8}T^3 \quad R^2 = 0.991 \quad (11)$$

$$NS1 - B0: f_C^T/f_C = 99.14 + 0.034T - 2.24 \times 10^{-4}T^2 + 1.31 \times 10^{-7}T^3 \quad R^2 = 0.991 \quad (12)$$

$$NS1 - B0.1: f_C^T/f_C = 99.43 + 0.012T - 1.44 \times 10^{-4}T^2 + 6.82 \times 10^{-8}T^3 \quad R^2 = 0.981 \quad (13)$$

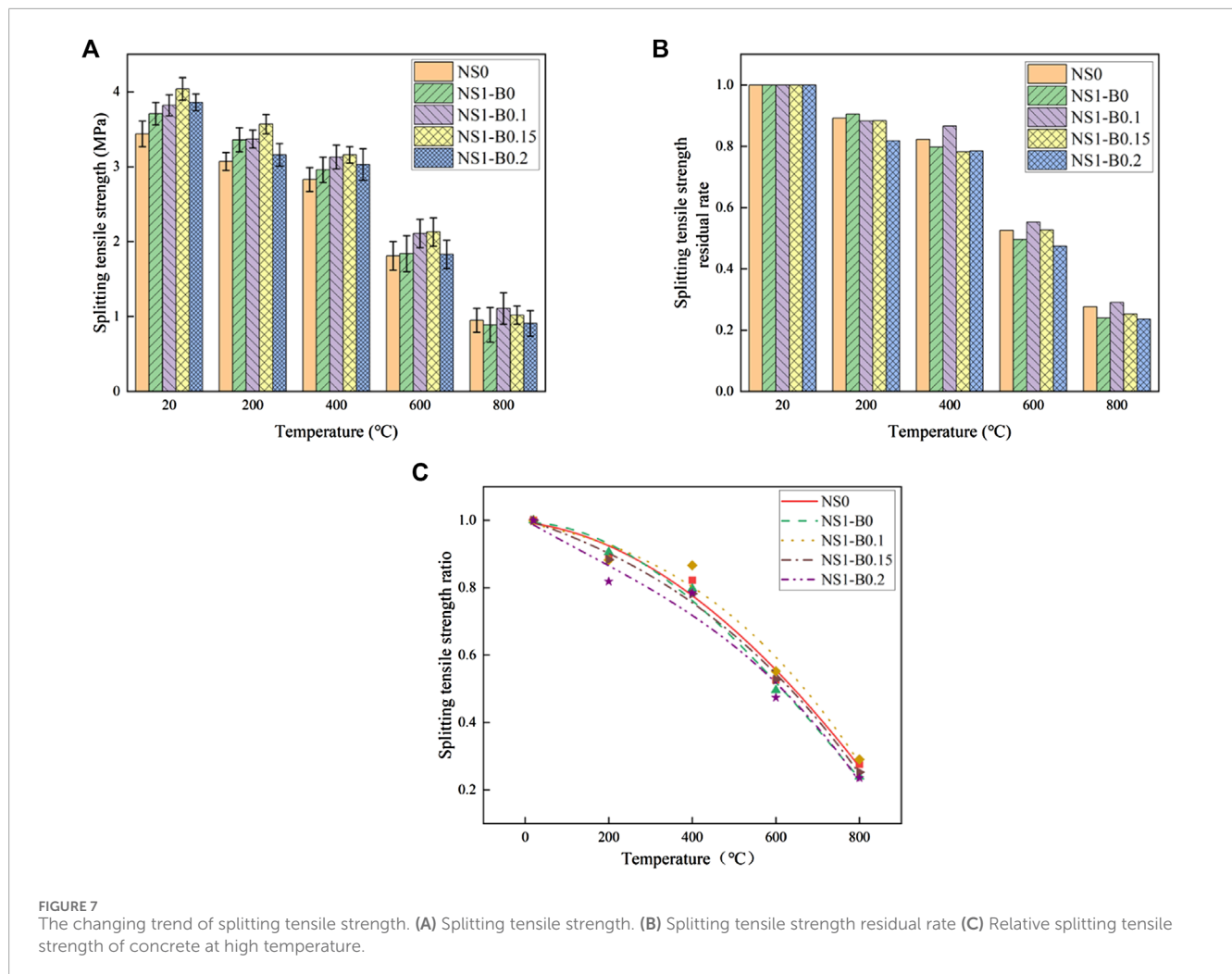
$$NS1 - B0.15: f_C^T/f_C = 99.40 + 0.018T - 1.64 \times 10^{-4}T^2 + 8.12 \times 10^{-8}T^3 \quad R^2 = 0.988 \quad (14)$$

$$NS1 - B0.2: f_C^T/f_C = 99.11 + 0.032T - 2.13 \times 10^{-4}T^2 + 1.23 \times 10^{-7}T^3 \quad R^2 = 0.986 \quad (15)$$

Where  $f_C^T$  (MPa) is the prism compressive strength of concrete after action temperature,  $f_C$  (MPa) is the prism compressive strength of concrete at 20°C,  $T$  (°C) is the temperature,  $R^2$  is the correlation coefficient.

### 3.5 Flexural strength

The flexural strength test results of the specimens after exposure to different high temperatures are presented in Table 4. Figures 9A,B illustrate the variation of flexural strength and flexural strength residual rate for each group of concrete with



temperature. From Figure 9A, it can be observed that the flexural strength of each group of concrete decreases with the increase in temperature. After adding NS, the flexural strength of the concrete was improved. After exposure to various temperatures, the flexural strength increased by 8.7%, 5.3%, 18.4%, 7.8%, and 4.3%, respectively, compared with plain concrete. This improvement was mainly attributed to the filling effect and volcanic ash effect of NS. At 20°C, the flexural strength of BF-NS concrete with fiber content of 0.10%, 0.15%, and 0.20% was 8.0%, 4.9%, and 2.9% higher than that of NS concrete, respectively; at 200°C, it increased by 12.9%, 6.1%, and 2.9%; at 400°C increased by 13.9%, 8.9%, and 2.2%; at 600°C, it increased by 33.3%, 16.4%, and 6.7%; at 800°C, it increased by 17.2%, 11.8%, and 8.9%. As a stress transfer medium, BF improved the ductility of concrete after cracking by forming a three-dimensional network structure inside the concrete to withstand high stress and then improved the flexural strength of NS concrete after high temperatures. Especially at 600°C, the flexural strength of NS concrete was significantly enhanced. Overall, after each temperature treatment, the BF with a content of 0.1% had a notable effect on the flexural strength of NS concrete.

As shown in Figure 9B, the residual rate of flexural strength decreases gradually with the increase of temperature under various temperature conditions. At 800°C, the residual flexural strength of plain concrete was only 36.2%, and that of NS concrete was only 34.7%. After experiencing high temperatures, BF-NS concrete exhibited good flexural capacity. Taking comprehensive consideration, the fiber content of 0.1% BF for NS concrete flexural capacity improvement was the most effective. After reaching temperatures beyond 800°C, the residual flexural strength exceeded that of NS concrete by 6.6%. The addition of BF introduced a small amount of air into the concrete, facilitating the dissipation of heat and mitigating strength loss at high temperatures. Consequently, the flexural strength's residual rate in concrete with BF surpassed that in both ordinary concrete and NS concrete.

By comparing the flexural strength of each concrete group after exposure to high temperatures with the strength at 20°C, the relationship curve depicting the flexural strength ratio with temperature was obtained. As illustrated in Figure 9C and Eqs (16–20), the fitting relationship between the flexural strength ratio of each concrete group and temperature can be discerned:

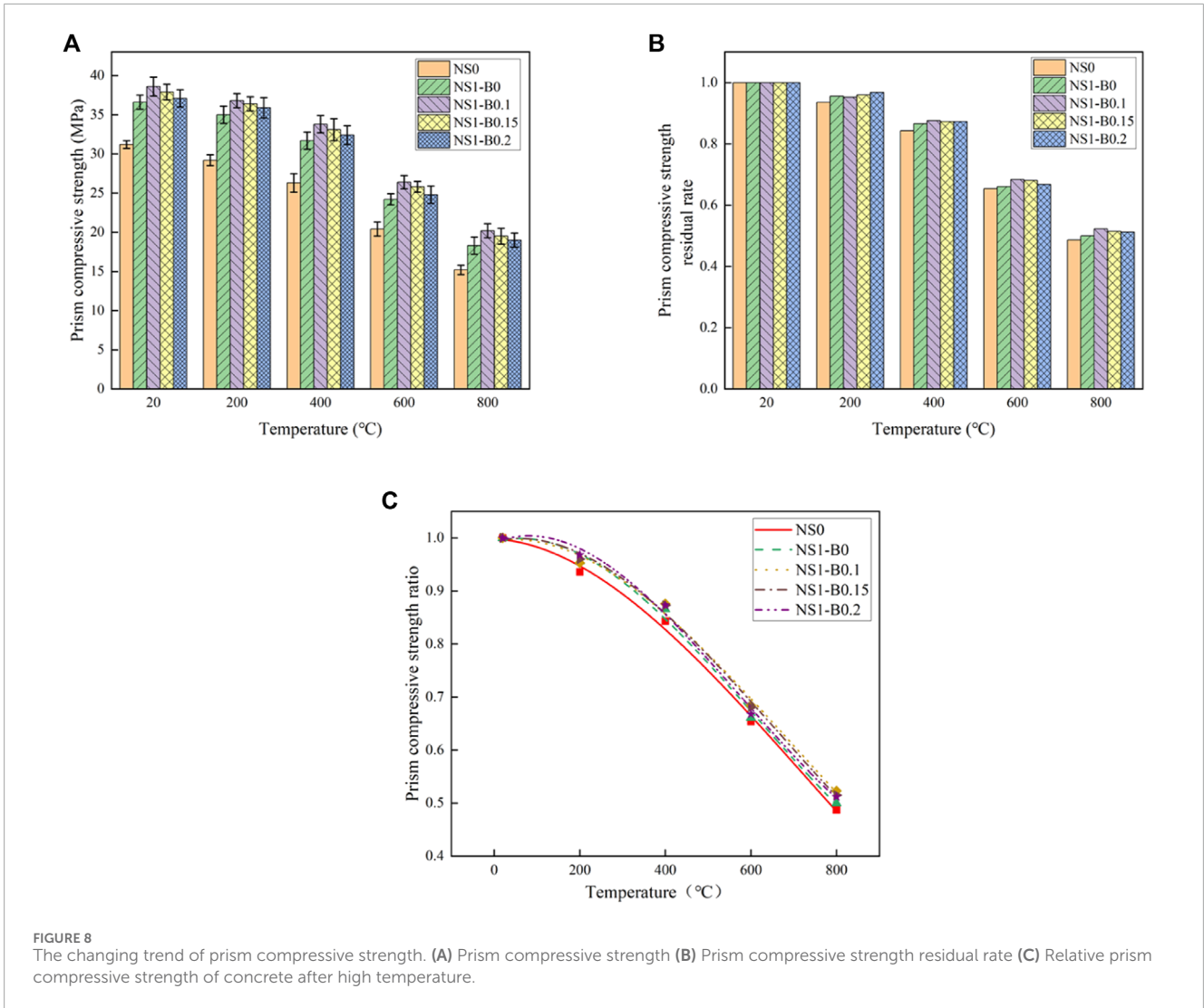


**FIGURE 8** The changing trend of prism compressive strength. (A) Prism compressive strength (B) Prism compressive strength residual rate (C) Relative prism compressive strength of concrete after high temperature.

$$NS0: f_C^T / f_C = 99.12 + 0.049T - 4.67 \times 10^{-4}T^2 + 3.84 \times 10^{-7}T^3 \quad R^2 = 0.999 \quad (16)$$

$$NS1 - B0: f_C^T / f_C = 98.46 + 0.042T - 4.04 \times 10^{-4}T^2 + 3.15 \times 10^{-7}T^3 \quad R^2 = 0.952 \quad (17)$$

$$NS1 - B0.1: f_C^T / f_C = 98.83 + 0.043T - 3.41 \times 10^{-4}T^2 + 2.40 \times 10^{-7}T^3 \quad R^2 = 0.985 \quad (18)$$

$$NS1 - B0.15: f_C^T / f_C = 98.42 + 0.044T - 3.78 \times 10^{-4}T^2 + 2.82 \times 10^{-7}T^3 \quad R^2 = 0.952 \quad (19)$$

$$NS1 - B0.2: f_C^T / f_C = 98.25 + 0.059T - 4.25 \times 10^{-4}T^2 + 3.18 \times 10^{-7}T^3 \quad R^2 = 0.964 \quad (20)$$

Where  $f_C^T$  (MPa) is the flexural strength of concrete after action temperature,  $f_C$  (MPa) is the flexural strength of concrete at 20°C,  $T$  (°C) is the temperature,  $R^2$  is the correlation coefficient.

### 3.6 Changes in the appearance of concrete

Upon exposure to different temperature effects, the appearance of each concrete group undergoes changes. Given the superior high-temperature resistance of the NS1-B0.1 group, its appearance is specifically analyzed. Figure 10 illustrates the changes in appearance of the NS1-B0.1 group concrete after exposure to varying temperature effects. From the figure, it is evident that at 20°C, the surface of the concrete exhibits a gray color, and the specimen appears intact. As the temperature rises to 200°C, the surface color of the concrete undergoes a slight change, transitioning from gray to yellow. However, the color change remains relatively minimal compared to the condition at 20°C, and there are no visible cracks on the surface of the test block. At 400°C, the surface color of the concrete darkens, and small cracks begin to appear. Upon reaching 600°C, the color of the concrete surface starts to lighten, accompanied by an increase in the number of small cracks on the specimen's surface. Finally, at 800°C, the surface color of the concrete

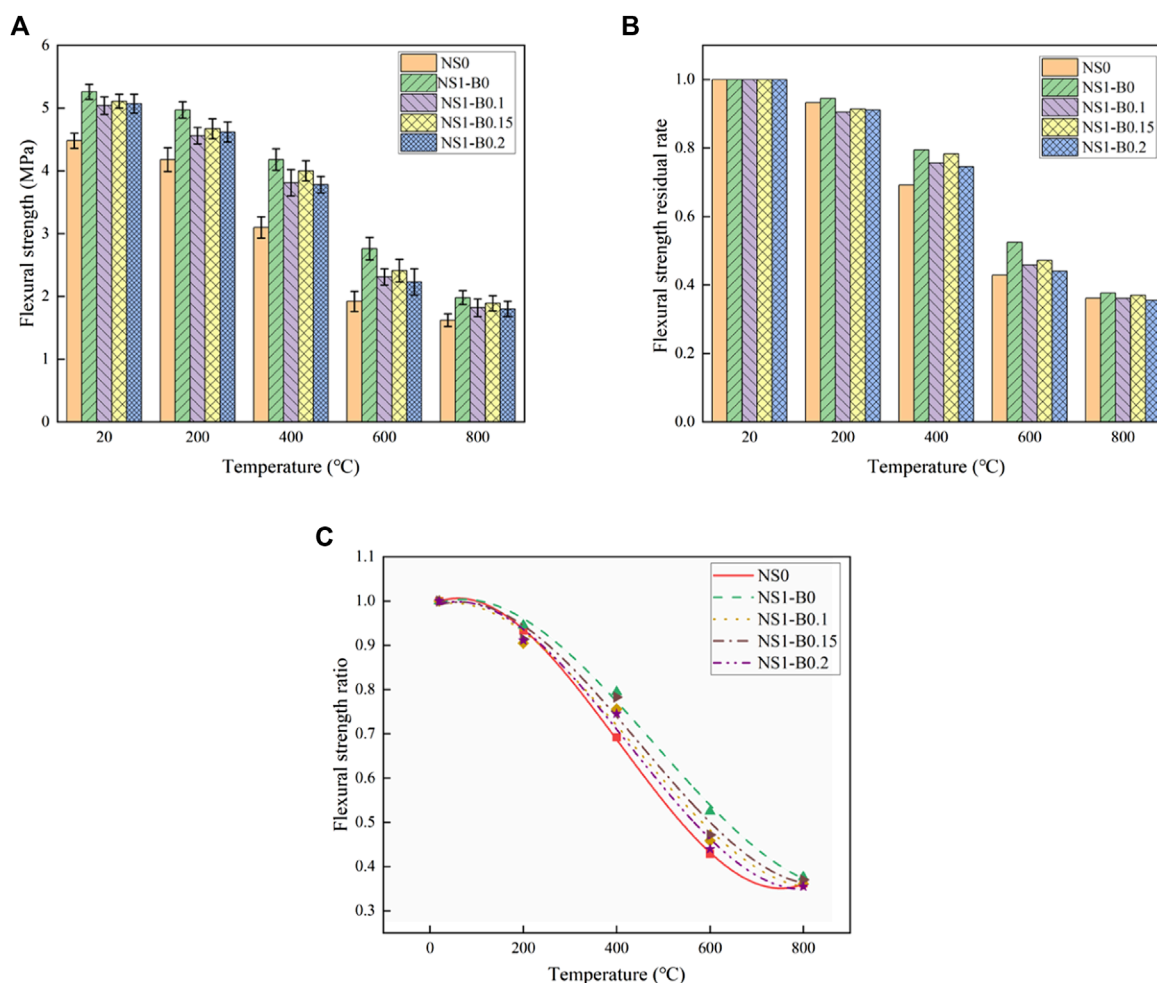


**FIGURE 9** The changing trend of flexural strength. (A) Flexural strength (B) Flexural strength residual rate (C). Relative flexural strength of concrete after high temperature.

becomes white, with numerous cracks visible on the surface.

### 3.7 Microstructure of NS1-B0.1

As the NS1-B0.1 group exhibits superior cubic compressive strength, prism compressive strength, and flexural strength, it is chosen for microstructure analysis. The microstructure of NS1-B0.1 at 20°C is depicted in Figure 11A. The concrete surface exhibited a small amount of CH crystals and a large amount of C-S-H gel, NS, and BF. The pozzolanic and filling effects of NS contributed to improved mortar compactness. Cement hydration produced CH crystals, which reacted with NS to form C-S-H gel. NS and C-S-H gel worked together to fill the internal voids of concrete, resulting in a more uniform and dense mortar. The microstructure of concrete was enhanced, leading to improved macroscopic mechanical properties. The anti-cracking and toughening effects of BF acted as a form of “secondary reinforcement” in the concrete, further enhancing

the mechanical properties of NS concrete. The pozzolanic and filling effects of NS resulted in more C-S-H gel adhering to the surface of BF, strengthening the bond between BF and cement paste.

The microstructure of NS1-B0.1 at 200°C is illustrated in Figure 11B. Post-200°C, both CH crystals and C-S-H gel remained intact, while capillary water and adsorbed water evaporated in the concrete. This led to the formation of voids and fine cracks in the uniform and dense continuous matrix, subsequently resulting in decreased splitting tensile strength, prism compressive strength, and flexural strength. The evaporated capillary water and adsorbed water reacted with unreacted cement particles, producing additional C-S-H gel to fill the cracks and voids. As a result, the compressive strength of the cubic showed a slight improvement at 200°C compared with 20°C. Due to the excellent hydrophilicity of BF (Krayushkina et al., 2019), it facilitated the interaction between the fiber and the cement matrix. Water molecules adsorbed onto the surface of BF and participated in the hydration reaction, leading to the production of more C-S-H gel on the surface of BF. This, in turn, enhanced the

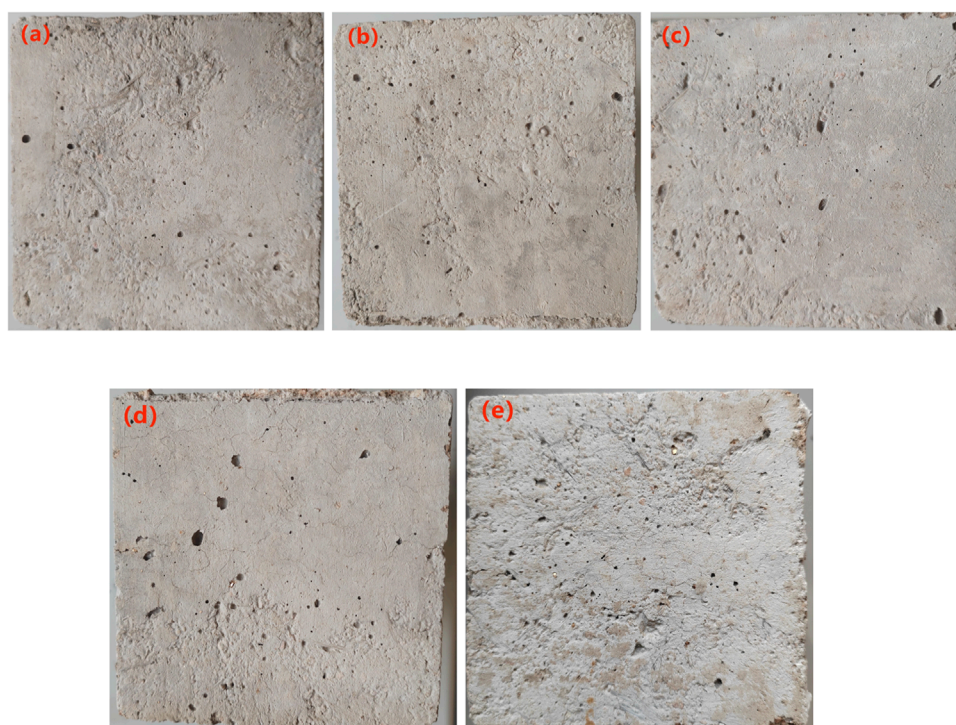


FIGURE 10 Apparent change of concrete NS1-B0.1 groups after different temperature (A) 20°C (B) 200°C (C) 400°C (D) 600°C (E) 800°C.

bond between the fiber and the matrix. BF did not break, and its surface exhibited slight wear, indicating that BF consistently bridged cracks until it was eventually pulled out.

The microstructure of NS1-B0.1 at 400°C is depicted in Figure 11C. As the temperature reached 400°C, coupled with the evaporation of water, the C-S-H gel remained intact while part of the CH crystal decomposed. The decomposition of the CH crystal led to a further increase in voids in the cement matrix and the continuous extension of small cracks. A gap emerged between BF and the cement matrix, diminishing the bonding performance between BF and the cement matrix, and ultimately deteriorated the mechanical properties.

The microstructure of NS1-B0.1 at 600°C is illustrated in Figure 11D. As the temperature reached 600°C, the CH crystal was entirely decomposed, and the C-S-H gel underwent partial decomposition. The cement matrix experienced noticeable volume shrinkage, resulting in the emergence of numerous voids and cracks. The original internal structure of the concrete was disrupted, leading to a significant deterioration in the macroscopic mechanical properties. The gap between BF and the cement matrix widened, diminishing the bonding performance with the cement paste.

The microstructure of NS1-B0.1 at 800°C is depicted in Figure 11E. As the temperature reached 800°C, the C-S-H gel underwent complete decomposition, and the voids and cracks within the cement matrix continued to increase. The internal structure of the concrete experienced more severe damage. Due

to the continued widening of the gap between BF and the cement matrix, along with the complete decomposition of the C-S-H gel on the surface of BF, the bonding force between BF and the cement matrix became nearly ineffective, leading to a serious deterioration in mechanical properties.

The aforementioned alterations demonstrated that high temperatures had a minimal impact on BF, and BF could effectively mitigate cracks in the concrete matrix under elevated temperatures. Additionally, it imparted a toughening effect on the concrete, preventing the concrete from spalling under high temperatures. Consequently, BF-NS concrete retained a relatively high residual strength even in high-temperature conditions.

## 4 Conclusion

- (1) As the temperature rises, the surface cracks of plain concrete, NS concrete, and BF-NS concrete progressively intensify, accompanied by a gradual increase in the mass loss rate. Plain concrete experiences a gradual decrease in cubic compressive strength with rising temperatures. In contrast, both NS concrete and BF-NS concrete exhibit an initial increase followed by a subsequent decline in cubic compressive strength as temperature changes. The cubic compressive strength of each concrete group peaks at 200°C. Post-

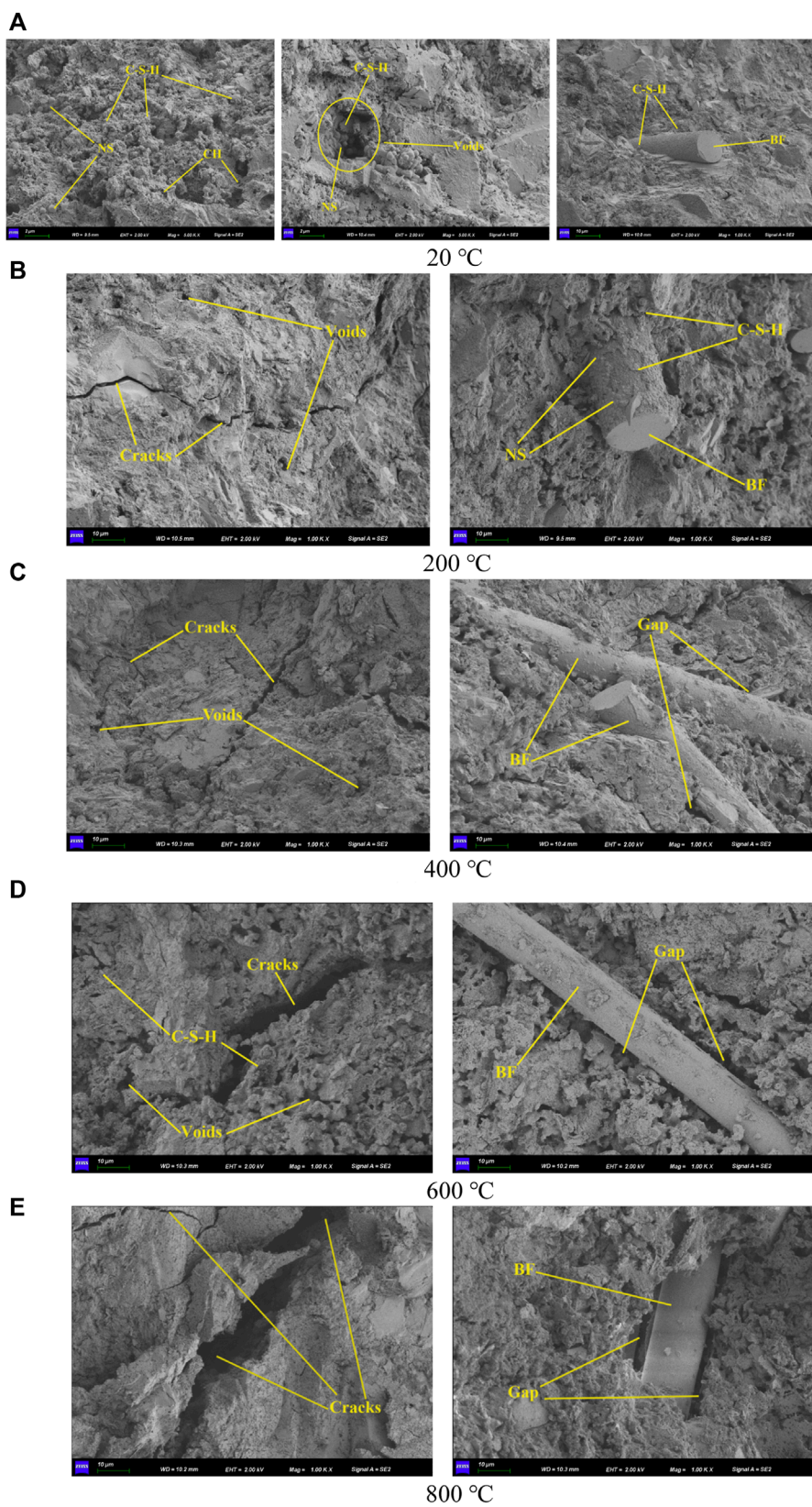


FIGURE 11 Microstructure of NS1-B0.1 (A) 20°C (B) 200°C (C) 400°C (D) 600°C (E) 800°C.

800°C, the residual cubic compressive strength of each group ranges from 47.4% to 59.2%. Notably, a BF content of 0.2% negatively impacts the cubic compressive strength of NS concrete.

- (2) As the temperature increases, the splitting tensile strength, prism compressive strength, and flexural strength of plain concrete, NS concrete, and BF-NS concrete all exhibit a gradual decline. The inclusion of NS enhances the splitting tensile strength, prism compressive strength, and flexural strength of plain concrete. Post-800°C, the residual rates for splitting tensile strength in NS concrete, prism compressive strength, and flexural strength are merely 24.5%, 50%, and 34.7%, respectively.
- (3) Considering all factors, a BF content of 0.15% yields the most significant enhancement in the splitting tensile strength of NS concrete. After exposure to 800°C, the splitting tensile strength is 13.5% higher than that of NS concrete, with a residual strength rate 14.6% superior to that of NS concrete. For improving the prism compressive capacity of NS concrete, a BF content of 0.1% demonstrates the most effective improvement. After exposure to 800°C, the prism compressive strength is 10.4% higher than that of NS concrete, and the residual strength rate increases by 2.3%. Similarly, a BF content of 0.1% offers the most substantial improvement in the flexural capacity of NS concrete. After exposure to 800°C, the flexural strength increases by 17.2% compared to NS concrete, with a residual strength rate 6.6% higher.
- (4) Through the analysis of experimental data, we establish a fitting relationship between the ratios of concrete cubic compressive strength, splitting tensile strength, prism compressive strength, flexural strength, and temperature. This provides a theoretical reference for further research on the mechanical properties of BF-NS concrete after exposure to high temperatures.

## References

- Abhilash, A., Nayak, D. K., Sangoju, B., Kumar, R., and Kumar, V. (2021). Effect of nano-silica in concrete; a review. *Constr. Build. Mater.* 278, 122347. doi:10.1016/j.conbuildmat.2021.122347
- Alaskar, A., Albidah, A., Alqarni, A. S., Alyousef, R., and Mohammadhosseini, H. (2021). Performance evaluation of high-strength concrete reinforced with basalt fibers exposed to elevated temperatures. *J. Build. Eng.* 35, 102108. doi:10.1016/j.jobbe.2020.102108
- Ashokan, A., Rajendran, S., and Dhairiyasamy, R. (2023). A comprehensive study on enhancing the mechanical properties of steel fiber-reinforced concrete through nano-silica integration. *Sci. Rep.* 13 (1), 20092. doi:10.1038/s41598-023-47475-0
- Ayub, T., Shafiq, N., and Nuruddin, M. F. (2014). Mechanical properties of high-performance concrete reinforced with basalt fibers. *Procedia Eng.* 77, 131–139. doi:10.1016/j.proeng.2014.07.029
- Bastami, M., Baghbadrani, M., and Aslani, F. (2014). Performance of nano-Silica modified high strength concrete at elevated temperatures. *Constr. Build. Mater.* 68, 402–408. doi:10.1016/j.conbuildmat.2014.06.026
- Cai, Y., Hou, P., Cheng, X., Du, P., and Ye, Z. (2017). The effects of nanoSiO<sub>2</sub> on the properties of fresh and hardened cement-based materials through its dispersion with silica fume. *Constr. Build. Mater.* 148, 770–780. doi:10.1016/j.conbuildmat.2017.05.091
- Cheng, T. H., and Li, Y. X. (2017). Study on mechanical performance of basalt fiber reinforced concrete. *China Concr. Cem. Prod.* (01), 53–56.
- Dias, D. P., and Thaumaturgo, C. (2005). Fracture toughness of geopolymeric concretes reinforced with basalt fibers. *Cem. Concr. Compos.* 27 (1), 49–54. doi:10.1016/j.cemconcomp.2004.02.044
- Ding, W., and Leng, F. G. (2011) “JGJ 55-2011,” in *Specification for mix proportion design of ordinary concrete*. Beijing, China: Chinese Standard Press.
- Forty, A. (2012). *Concrete and Culture: a material history*. London: Reaktion Books.
- High, C., Seliem, H. M., El-Safy, A., and Rizkalla, S. H. (2015). Use of basalt fibers for concrete structures. *Constr. Build. Mater.* 96, 37–46. doi:10.1016/j.conbuildmat.2015.07.138
- Huang, C. K., and Zhao, S. B. (2010). *CECS 13-2009. Standard test methods for fiber reinforced concrete*. Beijing, China: Chinese Standard Press.
- Huang, G. L., Sun, Z. J., Wang, M. C., and Zhang, Z. G. (2006). Experimental research on mechanical properties of basalt fiber and composites. *Compos. Sci. Eng.* (01), 24–27.
- Krayushkina, K., Khymeryk, T., and Bieliatynskiy, A. (2019). Basalt fiber concrete as a new construction material for roads and airfields. *IOP Conf. Ser. Mater. Sci. Eng.* 708, 012088. doi:10.1088/1757-899X/708/1/012088
- Lal, H. M., Uthaman, A., Li, C., Xian, G., and Thomas, S. (2022). Combined effects of cyclic/sustained bending loading and water immersion on the interface shear strength of carbon/glass fiber reinforced polymer hybrid rods fordoi:10.1016/j.conbuildmat.2021.125587

## Data availability statement

The original contributions presented in the study are included in the article/Supplementary Material, further inquiries can be directed to the corresponding author.

## Author contributions

WY: Writing–original draft, Conceptualization, Formal Analysis, Methodology, Validation, Visualization. HL: Writing–review and editing, Data curation, Funding acquisition, Project administration, Software, Validation. HW: Writing–review and editing, Investigation, Resources.

## Funding

The author(s) declare that no financial support was received for the research, authorship, and/or publication of this article.

## Conflict of interest

The authors declare that the research was conducted in the absence of any commercial or financial relationships that could be construed as a potential conflict of interest.

## Publisher's note

All claims expressed in this article are solely those of the authors and do not necessarily represent those of their affiliated organizations, or those of the publisher, the editors and the reviewers. Any product that may be evaluated in this article, or claim that may be made by its manufacturer, is not guaranteed or endorsed by the publisher.

- León, N., Massana, J., Alonso, F., Moragues, A., and Sánchez-Espinosa, E. (2014). Effect of nano-SiO<sub>2</sub> and nano-Al<sub>2</sub>O<sub>3</sub> on cement mortars for use in agriculture and livestock production. *Biosyst. Eng.* 123, 1–11. doi:10.1016/j.biosystemseng.2014.04.009
- Li, C., and Xian, G. (2019). Experimental and modeling study of the evolution of mechanical properties of PAN-based carbon fibers at elevated temperatures. *Materials* 12 (5), 724. doi:10.3390/ma12050724
- Li, R., Hou, P., Xie, N., Ye, Z., Cheng, X., and Shah, S. P. (2018). Design of SiO<sub>2</sub>/PMHS hybrid nanocomposite for surface treatment of cement-based materials. *Cem. Concr. Compos.* 87, 89–97. doi:10.1016/j.cemconcomp.2017.12.008
- Ling, Y., Zhang, P., Wang, J., and Chen, Y. (2019). Effect of PVA fiber on mechanical properties of cementitious composite with and without nano-SiO<sub>2</sub>. *Constr. Build. Mater.* 229, 117068. doi:10.1016/j.conbuildmat.2019.117068
- Lu, Y., Lu, J. T., He, X. F., Cao, X. X., and Qing, P. L. (2013). Research progress on preparation and effect on cement hydration of nano silica. *Bull. Chin. Ceram. Soc.* (07), 1335–1339.
- Mastali, M., Dalvand, A., and Sattarifar, A. R. (2016). The impact resistance and mechanical properties of reinforced self-compacting concrete with recycled glass fibre reinforced polymers. *J. Clean. Prod.* 124, 312–324. doi:10.1016/j.jclepro.2016.02.148
- Mohseni, E., Naseri, F., Amjadi, R., Khotbehsara, M. M., and Ranjbar, M. M. (2016). RETRACTED: microstructure and durability properties of cement mortars containing nano-TiO<sub>2</sub> and rice husk ash. *Constr. Build. Mater.* 114, 656–664. doi:10.1016/j.conbuildmat.2016.03.136
- Mukharjee, B. B., and Barai, S. V. (2014). Influence of Nano-Silica on the properties of recycled aggregate concrete. *Constr. Build. Mater.* 55, 29–37. doi:10.1016/j.conbuildmat.2014.01.003
- Nigam, M., and Verma, M. (2023). Effect of nano-silica on the fresh and mechanical properties of conventional concrete. *Forces Mech.* 10, 100165. doi:10.1016/j.finmec.2022.100165
- Norhasri, M. S. M., Hamidah, M. S., and Fadzil, A. M. (2017). Applications of using nano material in concrete: a review. *Constr. Build. Mater.* 133, 91–97. doi:10.1016/j.conbuildmat.2016.12.005
- Piao, Z. D. (2017). *Experimental study on mechanical properties of basalt fiber reinforced concrete after high temperature*. China: Zhengzhou University. MS thesis.
- Qin, Y. W. (2021). *Study on durability of basalt fiber reinforced concrete after high temperature*. China: China University of Mining and Technology. MS thesis.
- Qiu, G. Z., Fang, J. H., Xu, A. H., Wang, Q. Z., Jiang, S., and Li, H. (2019). Research on high-temperature performance of basalt fiber asphalt concrete. *Bull. Chin. Ceram. Soc.* (12), 3890–3896.
- Rong, J. W., Lu, J., and Yao, W. (2002). *Gb/t 50081-2002. Standard for test method of mechanical properties on ordinary concrete*. Shenzhen, China: Chinese Standard Press.
- Rong, H. R., Wang, H. L., Chu, S. H., Liang, Y. Z., and Zhi, Z. L. (2020). Study on mechanical properties of basalt fiber reinforced concrete under high temperature. *Fly. Ash Compr. Util.* (01), 56–60.
- Shih, J. Y., Chang, T. P., and Hsiao, T. C. (2006). Effect of nanosilica on characterization of Portland cement composite. *Mater. Sci. Eng. A* 424 (1), 266–274. doi:10.1016/j.msea.2006.03.010
- Sikora, P., Abd Elrahman, M., and Stephan, D. (2018). The influence of nanomaterials on the thermal resistance of cement-based composites—a review. *Nanomaterials* 8 (7), 465. doi:10.3390/nano8070465
- Sim, J., Park, C., and Moon, D. Y. (2005). Characteristics of basalt fiber as a strengthening material for concrete structures. *Compos. Part B Eng.* 36 (6), 504–512. doi:10.1016/j.compositesb.2005.02.002
- Sun, G. D., Jiao, H. Z., Chen, X. M., Han, Z. Y., and Li, S. J. (2018). Reinforcing effect and mechanism of chopped basalt fiber on concrete. *Ind. Constr.* (01), 118–121+183.
- Sun, H., Luo, L., Yuan, H., and Li, X. (2023). Experimental evaluation of mechanical properties and microstructure for recycled aggregate concrete collaboratively modified with nano-silica and mixed fibers. *Constr. Build. Mater.* 403, 133125. doi:10.1016/j.conbuildmat.2023.133125
- Swolfs, Y., Gorbatikh, L., and Verpoest, I. (2014). Fibre hybridisation in polymer composites: a review. *Compos. Part A Appl. Sci. Manuf.* 67, 181–200. doi:10.1016/j.compositesa.2014.08.027
- Uthaman, A., Lal, H. M., Li, C., Xian, G., and Thomas, S. (2021). Mechanical and water uptake properties of epoxy nanocomposites with surfactant-modified functionalized multiwalled carbon nanotubes. *Nanomaterials* 11 (5), 1234. doi:10.3390/nano11051234
- Wang, X. T., Zhou, M., and Wang, W. Z. (2012). Experimental study of fire response and post-fire mechanical performance of profiled sheet-ceramsite concrete composite floor. *J. Build. Struct.* 33, 10–17.
- Wang, Y., Hughes, P., Niu, H., and Fan, Y. (2019). A new method to improve the properties of recycled aggregate concrete: composite addition of basalt fiber and nano-silica. *J. Clean. Prod.* 236, 117602. doi:10.1016/j.jclepro.2019.07.077
- Xiao, J. Z., Li, B., Zhang, K. J., Su, Y. W., and Pan, Y. P. (2021). Dynamic mechanical properties of nano-silica modified recycled aggregate concrete under uniaxial compression. *J. Tongji Univ. Sci.* (01), 30–39.
- Yan, L., and Xing, Y. M. (2013). Influence of nano-SiO<sub>2</sub> on mechanical properties and microstructure of steel fiber reinforced concrete after heating at high temperatures. *Acta Mater. Compos. Sin.* (03), 133–141.
- Yang, L., Lü, J., Xie, H., Yang, D., Fan, P., Li, J., et al. (2023). Experimental study on uniaxial compressive properties and damage evolution of basalt fiber reinforced concrete after being subjected to high temperature. *Structures* 54, 693–703. doi:10.1016/j.istruc.2023.05.089
- Zhang, X. Y., and Xie, S. D. (2022). *Gb 14685-2022. Pebble and crushed stone for construction*. Beijing, China: Chinese Standard Press.
- Zhang, T., Zhang, Y., Xiao, Z., Yang, Z., Zhu, H., Ju, J. W., et al. (2019). Development of a novel bio-inspired cement-based composite material to improve the fire resistance of engineering structures. *Constr. Build. Mater.* 225, 99–111. doi:10.1016/j.conbuildmat.2019.07.121
- Zhang, J., Liu, H., Liu, G., Wang, X., Geng, J., Wang, Q., et al. (2023). Influence on mechanical properties and microstructure analysis of hybrid fiber recycled aggregate concrete after exposure to elevated temperature. *J. Adhesion Sci. Technol.* 37 (16), 2328–2347. doi:10.1080/01694243.2022.2127251
- Zhao, Y. R., Liu, D. K., Wang, L., and Liu, F. F. (2019). Experimental study on mechanical properties of basalt fiber concrete after high temperature. *Concrete* (10), 72–75.
- Zheng, Y., Zhuo, J., and Zhang, P. (2021). A review on durability of nano-SiO<sub>2</sub> and basalt fiber modified recycled aggregate concrete. *Constr. Build. Mater.* 304, 124659. doi:10.1016/j.conbuildmat.2021.124659
- Zhu, Y., and Ma, Q. Y. (2016). Experiment research on compressive and tensile strength of nano-SiO<sub>2</sub> concrete with basalt fiber. *Sci. Technol. Eng.* (11), 240–243+248.